Colloids and Surfaces B: Biointerfaces 196 (2020) 111321

Contents lists available at ScienceDirect

Colloids and Surfaces B: Biointerfaces

journal homepage: www.elsevier.com/locate/colsurfb

An Improved Substrate for Superior Imaging of Individual Biomacromolecules with Atomic Force Microscopy

Dmitry V. Klinov[a,1], Anna D. Protopopova[b,1], Dmitry S. Andrianov[c], Rustem I. Litvinov[b,d], John W. Weisel[b,*]

[a] Federal Research and Clinical Center of Physical-Chemical Medicine, Moscow, Russian Federation
[b] Department of Cell and Developmental Biology, University of Pennsylvania School of Medicine, Philadelphia, PA, USA
[c] Department of Biochemistry and Biophysics, University of Pennsylvania School of Medicine, Philadelphia, PA, USA
[d] Institute of Fundamental Medicine and Biology, Kazan Federal University, Kazan, Russian Federation

ARTICLE INFO

Keywords:
Atomic force microscopy
Highly oriented pyrolytic graphite
Graphite modification
Proteins
Nucleic acids
Polysaccharides

ABSTRACT

High-resolution atomic force microscopy (AFM) of biomacromolecules is a valuable method for structural studies in biology. Traditionally, the surfaces used for AFM imaging of individual molecules are limited to mica, graphite, and glass. Because these substrates have certain shortcomings, new or modified surfaces that improve the quality of AFM imaging are highly desirable. Here, we describe an improved substrate for imaging of individual biomacromolecules with high-resolution AFM based on graphite surfaces coated by physical adsorption. We provide a detailed methodology, including the chemical structure, synthesis, characterization and the use of a substance that modifies the surface of freshly cleaved graphite, making it suitable for adsorption and AFM visualization of various biomacromolecules while minimizing spatial distortions. We illustrate the advantages of the modified graphite over regular surfaces with examples of high-resolution single-molecule imaging of proteins, polysaccharides, DNA and DNA-protein complexes. The proposed methodology is easy to use and helps to improve substantially AFM imaging of biomacromolecules of various natures, including flexible and/or unstructured sub-molecular regions that are not seen on other AFM substrates. The proposed technique has the potential to improve the use of AFM in structural biology for visualization and morphometric characterization of macromolecular objects.

1. Introduction

Atomic force microscopy (AFM) has become a versatile methodology with numerous applications in many fields of research and development. In particular, it has been widely used in molecular biology and related fields to visualize individual molecules of biopolymers, such as proteins, nucleic acids, and polysaccharides [1]. The basic imaging modes of AFM provide 3D topography images of the sample surface with a high spatial resolution, typically reaching 5-20 nm in the X-Y plane and about 0.1 nm in height, corresponding to molecular and submolecular dimensions. Further increasing the quality and reproducibility of single-molecule images is one of the main avenues of research for modern AFM.

There are a number of preconditions that determine the resolution and quality of AFM-based molecular imaging, of which sharpness of the tip and quality of the substrate are perhaps the most critical. Of course, the atomic smoothness of an adsorptive substrate is important for a high-resolution AFM imaging; however, it is less well known that there are other significant properties of the substrate, such as a charge and hydrophobicity. As a result of empirical selection over the years, the number of substrates used for AFM imaging of biomacromolecules is rather limited. The most widely used substrate is mica, which is a negatively charged natural crystal with variable chemical structure and high wettability. The most important advantage of mica is that it could be easily cleaved to provide atomically smooth surfaces with no crystal steps for hundreds of micrometers. Mica is suitable for single-molecule visualization of proteins [2–4], DNA [5–7], and polysaccharides [8–11], but it is prone to imaging artifacts due to a high surface charge and absorption of water vapor from air [12,13]. Frequently used methods of mica functionalization with alkoxysilanes, including 3-aminopropyl-trietoxy silane (APTES), provide smooth positively charged surfaces suitable for visualization of nucleic acids and proteins

* Corresponding author at: Room 1154, BRB II/III, 421 Curie Boulevard, Philadelphia, PA 19104-6058, USA.
E-mail address: weisel@pennmedicine.upenn.edu (J.W. Weisel).
[1] These authors contributed equally.

https://doi.org/10.1016/j.colsurfb.2020.111321
Received 16 March 2020; Received in revised form 7 August 2020; Accepted 11 August 2020
Available online 16 August 2020
0927-7765/

[6,7].

Another frequently used substrate is *h*ighly *o*riented *p*yrolytic *g*raphite (HOPG), a chemically inert synthetic carbon crystal. It can be cleaved in the same manner as mica, but it is less uniformly flat because it has many more crystal steps per surface area. Moreover, bare graphite is known to induce conformational changes in adsorbed protein molecules [14–17]. To improve its surface properties, graphite has been modified by low-energy plasma [18] or by adsorption of long chain alkanes, alcohols, and fatty acids [19] to make it suitable for single-molecule imaging of proteins and DNA [20,21]. However, these modifications increase the roughness of graphite and long chain alkanes, alcohols, and fatty acids produce visible lamellar patterns on the surface.

Polished or chemically etched surfaces, such as silica and glass, are used less often than mica and graphite due to the high surface roughness that precludes visualization of fine structural details of adsorbed molecules. However, these surfaces are still practical for single-molecule AFM imaging of membrane proteins in lipid bilayers or some single protein molecules directly adsorbed on the substrate surface [22,23].

With a limited number of appropriate AFM substrates, new surfaces that allow for reproducible high-resolution AFM imaging of various biomacromolecules are highly desirable. Here, we describe the chemical structure, synthesis, and the use of a substance named a graphite modifier (GM) that coats the graphite surface and improves substantially AFM imaging of individual biomacromolecules. Graphite coated with GM enabled us to visualize sub-molecular elements, such as long and flexible unstructured regions in proteins, which are not observable in AFM with other surfaces. The method proposed to improve single-molecule AFM imaging is remarkably reproducible and universal to visualize proteins, nucleic acids, and polysaccharides. We describe in detail all stages needed to reproduce this methodology, including synthesis of the graphite modifier, coating of graphite, and preparation of biomolecular samples followed by their AFM imaging. We illustrate the advantages of the modified graphite over regular surfaces with examples of high-resolution single-molecule visualization of proteins, polysaccharides, DNA, and their complexes.

2. Experimental

2.1. Materials

N-methylmorpholine, 2-chloro-4,6-dimethoxy-1,3,5-triazine, 1,10-diaminodecane, and dimethyl sulfoxide (DMSO) for general laboratory use were purchased from Sigma-Aldrich (USA). *N*-Boc-tetraglycine was purchased from Genscript (USA) and was 98% pure by HPLC. Lyophilized human fibrinogen was from HYPHEN Biomed (France), lyophilized calf thymus DNA from Sigma-Aldrich (USA), and unfractionated heparin solution was from Becton Dickinson (USA). Human IgG was purified from serum of healthy donors as described [24] and was 98% pure by SDS-PAGE. We used a buffer containing 20 mM HEPES pH 7.4, 150 mM NaCl with or without addition of 5 mM $CaCl_2$ to dilute samples for AFM. Highly oriented pyrolytic graphite was from Electron Microscopy Sciences (USA).

NMR. ^{1}H NMR spectra were recorded on a Bruker DPX-400 spectrometer (400 MHz) at 298 K using DMSO-d_6 (Cambridge Isotope Laboratories, USA) as a solvent. The signals' resonance positions on ^{1}H NMR spectra are given as chemical shifts (in ppm) and were calibrated against the solvent residual peak (2.50 ppm).

2.2. Traditional substrates: mica and glass

We have tested three commonly used substrate surfaces: glow-discharged glass, freshly cleaved mica, and mica modified with (3-aminopropyl)triethoxysilane (APTES, Sigma-Aldrich, USA). To prepare glow-discharged glass, microscope cover glass slip (22 × 22 x 0.16 mm, Fisher Scientific, USA) was washed with a detergent, rinsed with 70v/v % ethyl alcohol, dried, and cleaned for 10 min using PDC-32G-2 Plasma Cleaner (Harrick Plasma, USA). Untreated mica was cleaved with a sticky tape and immediately used for sample preparation. APTES-modified mica was prepared by treatment of freshly cleaved mica with a diluted water solution of APTES [25].

2.3. Sample preparation on traditional AFM substrates

Proteins were diluted to 1-3 μg/ml concentration with a buffer (20 mM HEPES, pH 7.4, containing 150 mM NaCl and 5 mM $CaCl_2$). For deposition of proteins on the unmodified and modified mica, a 10-μl drop was put on a clean parafilm and a substrate was placed on top of it for 1 minute. Then the sample was washed with four 100-μl drops of fresh milli-Q water, the liquid remaining after the last washing step was blown away with a flow of air, making the surface dry and ready for imaging. To prepare protein samples on glass, 10 μl of a sample was deposited directly on the glass for 1 minute, rinsed with 500 μl of fresh milli-Q water, and dried with a flow of air.

2.4. AFM modes and tips

All images of biomolecules presented in this paper were obtained using a MFP-3D microscope (Asylum Research – Oxford Instruments, USA) pre-calibrated with an interferometer and verified using a calibration grid with 200-nm pits. Imaging was performed in air in tapping mode with a typical scan rate of 0.5 Hz, using rectangular silicon cantilevers OMCL-AC200TS (Olympus, Japan). Dimensions of the cantilever 200 × 40 × 3.5 μm, resonance frequency 150 ± 50 kHz, typical spring constant 9 N/m and characteristic tip radius 7 nm were provided by the manufacturer. Tapping mode imaging was performed with small operational amplitudes: the free amplitude was set at 100 mV, which corresponds to ~8 nm, the set-point amplitude was kept as high as possible for stable imaging in the attractive regime, and a typical set-point amplitude was equal to 50-70 mV.

The image showing the molecular arrangement of a GM layer on graphite was obtained using a Ntegra Prima microscope (NT-MDT, Russia) pre-calibrated with an interferometer and verified using a calibration grid with 20-nm pits. Imaging was performed in air in tapping mode with a scan rate of 0.5 Hz, using a super-sharp AFM cantilever that was made in-house by growing carbon nanoneedles at the tip of a standard commercially available silicon cantilever [26]. The super-sharp cantilever had a resonance frequency of 150 ± 50 kHz, a typical spring constant of 9 N/m, and a carbon nanoneedle tip radius of about 1 nm as measured by the transmission electron microscope [26]. The ultimate spatial resolution was obtained in the repulsive tip–sample interaction regime with small operational amplitudes: the free amplitude was set at 3-5 nm, the set-point amplitude was kept below 1 nm at the value which allowed for stable imaging in the repulsive regime.

2.5. AFM image analysis

FemtoScan Online software (http://www.femtoscanonline.com) [27] was used to filter, analyse, and present the AFM images. SPM Image Magic software (https://sites.google.com/site/spmimagemagic) was used for a semi-automatic measurement of the height of visualized molecules.

3. Results and Discussion

3.1. Chemical structure, synthesis, and characterization of the graphite modifier (GM)

The chemical name of GM is *N,N'*-(decane-1,10-diyl)bis(tetraglycineamide) dihydrochloride and its chemical structure is presented on Fig. 1. The molecule, which is one of a class of amphiphilic modifiers of hydrophobic surfaces [28], consists of a hydrophobic hydrocarbon

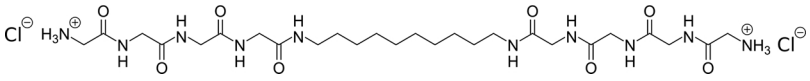

Fig. 1. Chemical structure of the graphite modifier *N,N'*-(decane-1,10-diyl)bis(tetraglycineamide) dihydrochloride. Synthesized as a dihydrochloride salt. In aqueous solutions, chloride ions exchange with other anions.

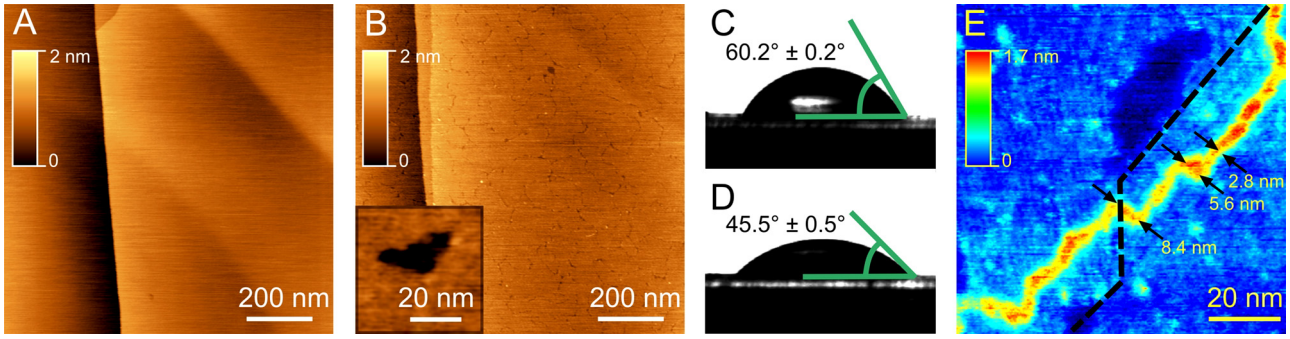

Fig. 2. Imaging and physical characterization of unmodified and GM-modified graphite surfaces. AFM images characterizing roughness and morphology of bare (A) and GM-coated (B) graphite. Image size 1 μm x 1 μm. Insert in B shows a typical crack in the layer of GM. Water contact angles measured on freshly cleaved bare graphite (C) and on freshly prepared GM-coated graphite (D). Each angle was calculated from 3 measurements on 3 independent samples. High-resolution AFM image of the lamellar structure of GM layer with a DNA molecule adsorbed along the lamellae (E). Image size 90 nm x 90 nm. Arrows point to the discrete steps that DNA makes between the neighboring lamellae. A dashed line indicates the boundary between two lamellar domains.

part ($C_{10}H_{20}$), which drives its adsorption to graphite, flanked by polar tetraglycines at physiological pH bearing positively charged protonated amines on both sides. The oligoglycine parts of the molecule reduce hydrophobicity of the graphite surface and promote adsorption of polar and negatively charged biomacromolecules via hydrogen bonds and electrostatic interactions, respectively.

The following protocol has been developed to synthesize and purify GM (Supplemental Fig. S1).

1 Add *N*-methylmorpholine (144 μM, 1.6 eq.) to the solution of 2-chloro-4,6-dimethoxy-1,3,5-triazine (CDMT) (86.6 μM, 1 eq.) in anhydrous dimethyl sulfoxide (DMSO) for activation and stir for 15 min at room temperature.
2 Add *N*-Boc-tetraglycine (86.6 μM, 1 eq.) to the solution and stir for 30 min at room temperature.
3 Add 1,10-diaminodecane (36 μM, 0.4 eq.) and incubate the stirring mixture overnight at room temperature.
4 Remove the solvent under reduced pressure.
5 Suspend the remaining solid in a small amount of methanol, filter on a glass filter, wash with another portion of methanol and dry.
6 Transfer the product (a colorless solid) into a round-bottom flask, dissolve in anhydrous trifluoroacetic acid and stir for 2 hours at room temperature. Evaporate the solution under reduced pressure.
7 Dissolve the residue in deionized water. Filter the resulting turbid solution through a 0.45-μm syringe filter.
8 Precipitate the material by adjusting pH to ca. 9 and filter the solid on a glass filter.
9 Dissolve the precipitate in 2% hydrochloric acid and co-evaporate with toluene and methanol/isopropanol mixture to dryness.
10 Suspend in diethyl ether, filter and dry, leaving the product as a colorless dihydrochloride salt.

GM is a colorless powder soluble in water as well as in dimethylformamide, DMSO, and methanol, and partially soluble in acetone. It is insoluble in methylene chloride, diethyl ether, tetrahydrofuran, and toluene. GM is rather stable at the room temperature, but for long-term storage it is advisable to keep it at +4-6 °C as a solid or a concentrated (1-2 mg/ml) stock solution.

The ^{1}H NMR spectra of the product recorded in deuterated DMSO (Supplemental Fig. S2) revealed characteristic peaks of amide protons (triplets at 8.72, 8.36, 8.10 and 7.79 ppm), the corresponding alkyl protons (doublets at 3.83, 3.75, 3.66, 3.61 ppm) of tetraglycine and a broad signal of the protonated amino groups (8.13 ppm), confirming the complete removal of the protecting groups. The structure was confirmed by the relative integral intensities of tetraglycine alkyl proton signals and C_{10} alkyl proton signals (3.02, 1.38, and 1.24 ppm). The high resolution mass spectra of GM revealed a molecular ion corresponding to the monoprotonated cation of GM (m/z found 629.3730, calculated 629.3729).

3.2. Preparation and physical characterization of GM-coated graphite

Before coating with GM to prepare an AFM substrate, highly oriented pyrolytic graphite is cleaved using one-sided sticky tape. Then a 9-μl drop of fresh milli-Q water is placed on the freshly cleaved graphite and 1 μl of 0.1 mg/ml water solution of GM is immediately added to a final concentration of 0.01 mg/ml, mixed thoroughly within the drop, incubated for 8 minutes, and dried by blowing air to make the surface ready for use.

The morphology and surface roughness of the GM-coated graphite were characterized with AFM in comparison with bare unmodified graphite (Fig. 2A). On a larger scale, the GM-coated graphite had a stepped surface that was indistinguishable from the bare graphite. On the zoomed images, a layer of the graphite modifier was discernible due to sparse surface defects or cracks 0.40 ± 0.05 nm (M ± SD, N = 100) in depth that did not affect the overall smoothness of the surface (Fig. 2B). Notably, we never observed adsorption of biomacromolecules within those defects, suggesting that they represent solvent-exposed non-covered graphite regions. The prevailing surface area of GM-coated graphite remained as smooth as bare graphite, the root mean square roughness (R_q) measured within flat parts of the graphite samples before or after coating with GM was equal to 0.09 ± 0.02 nm (M ± SD) as calculated from 10 images taken from three independently prepared samples of each type. Therefore, the modification did not affect the smoothness of the surface areas used for molecular imaging.

Next, we characterized the effect of GM on the hydrophobicity of graphite by measuring the water contact angle before and after coating. The measurements were done on an in-house built imaging system using a sessile drop method [29]. Bare, freshly cleaved graphite displayed an average water contact angle of 60.2° ± 0.2° (M ± SD, n = 3) (Fig. 2C), which is in agreement with the literature [30,31] and is characteristic of a relatively good wettability. After coating with GM, the average water contact angle went down to 45.5° ± 0.5° (M ± SD, n = 3) (Fig. 2D), showing that coating with GM rendered graphite more

wettable and hydrophilic than the bare graphite.

To study the molecular arrangement of the GM layer on graphite, we employed super-sharp AFM cantilevers with a tip radius of about 1 nm [26]. An AFM image of the fine structure of GM-modified graphite shows that the GM layer is composed of densely packed lamellae with a period of 2.8 nm (Fig. 2E). Formation of the ordered structure is caused by epitaxial crystallization of GM molecules on the surface of graphite. On the nanoscale, the molecules in the lamellae are densely packed parallel to the substrate and to each other. On a larger scale, lamellae form domains oriented along the hexagonal lattice of graphite and therefore often displaying a 60° angle between each other (Fig. 2E). The characteristic size of these domains is relatively large: from several hundred nanometers to micrometers, but under normal imaging conditions the lamellar pattern on GM-graphite is not visible due to its small period. DNA molecules adsorbed on the surface of GM-graphite allow for indirect observation of the lamellar structure because they are subjected to partial epitaxy and orient along the lamellae. The discrete steps that the DNA molecule makes between the neighboring lamellae to accommodate bending stress correspond to the period of the GM layer (Fig. 2E).

Although the exact atomic arrangement of a GM layer on graphite is unknown, we think that GM self-assembles in such a way that tetraglycines are exposed, making the surface highly hydrophilic, positively charged at pH 7.4, and thus readily adsorptive for various amphipathic, zwitterionic, and polyanionic biomacromolecules, comprising potential objects for AFM imaging.

3.3. Deposition of biomacromolecules on GM-graphite

The protocol of sample preparation on GM-coated graphite for AFM imaging is independent of the nature of biomacromolecules. For proteins, sulphated glycosaminoglycans, and nucleic acids, the protocol includes 3 consecutive steps.

1 Dilute macromolecule preparation to 1-3 μg/ml with an appropriate detergent-free buffer.
2 Apply 2 μl of the diluted sample on freshly prepared GM-coated graphite and let it remain for 5-15 s.
3 Take 20-100 μl of milli-Q water and add it carefully over the sample drop, keeping the mixed liquid for 5-15 s, and then remove it with a flow of air until the surface is dry and ready for imaging. It is important to keep adsorption (step 2) and rinsing (step 3) quick because prolonged exposure to the substrate may trigger unwanted conformational changes in the macromolecules, especially if the sample solution is non-physiological [14,32].

3.4. Applications of GM-coated graphite for imaging of individual protein molecules with high-resolution AFM

We used human blood proteins, immunoglobulin G (IgG) and fibrinogen, to demonstrate the advantages of GM-coated graphite for visualization of protein molecules over 3 other substrate surfaces commonly used for AFM of single biomacromolecules, namely glow-discharged glass, freshly cleaved mica, and mica modified with APTES.

3.4.1. AFM visualization of human IgG

IgG is a 150-kDa protein with a well-characterized 3D structure. Based on X-ray crystallography, IgG molecules typically have a Y-shape which measures approximately 12 nm x 12 nm x 4-5 nm [33]. Fig. 3A shows a representative image of individual IgG molecules on the GM-coated graphite substrate. The protein was distributed evenly on the sample surface with easily distinguishable single molecules and very few aggregates. Most of the IgG molecules appeared globular, while some had a characteristic Y-shape (Fig. 3B). When the same IgG preparation was adsorbed on other substrates used for comparison with GM-coated graphite, the IgG molecules had a similar appearance and were visualized as compact particles with a more or less pronounced Y-shape (Fig. 3C–E). However, the measured height values varied considerably depending on the substrate. On GM-coated graphite, the average apparent height of IgG was the largest and equaled 3.0 nm, compared to 2.1 nm on glass, 1.8 nm on bare mica, and 2.0 nm on APTES-mica (Fig. 3F–I). These dimensions suggest that on all the four surfaces analyzed, IgG molecules adsorb as flat structures and that the heights measured with AFM roughly correspond to the thickness of individual molecules determined crystallographically. The discrepancy of the AFM-based dimensions and crystal structures are unavoidable, due to surface effects upon adsorption of the protein molecules and sample drying that are typical for imaging of soft biomolecules by AFM. Additionally, in tapping mode the probe can interact differently with the macromolecules and their immediate surroundings as well as the macromolecules can be lying directly on the bare substrate or there might be an underlying "pillow" of surface adsorbate. However, the average IgG height value obtained on GM-coated graphite (3 nm) was the closest to the crystallographic dimensions (4-5 nm), suggesting that the protein structure is preserved on the GM-coated graphite better than on the other substrates tested.

3.4.2. AFM visualization of human fibrinogen

Fibrinogen is a 340-kDa glycoprotein that is essential for blood clotting, wound healing, inflammation, angiogenesis, and several other biological functions [34]. X-ray crystallographic studies show that this protein is a 45-nm rod-like molecule with three globular portions 3-5 nm in diameter connected by 17-nm-long α-helical coiled coils (Fig. S3) [34]. Fig. 4A shows a representative AFM image of fibrinogen on GM-coated graphite. The molecules were evenly distributed over the sample surface and clearly reproduced the overall crystal structure of fibrinogen: each molecule consisted of three globules with the distal globules being bigger than the central one, and all three globular portions connected by thin linkers. In addition to the compact folded core of the fibrinogen molecule, which is seen in X-ray crystallography, transmission electron microscopy, and AFM on various surfaces [3,35,36], using AFM on GM-coated graphite, we were able to visualize the long unstructured extended polypeptide chains called αC regions (Fig. S3) that showed up as thin flexible protrusions extending from the molecule (Fig. 4B) [37]. Also, with the use of the GM modifier we were able to distinguish the globular γ- and β-nodules located at the terminal regions of fibrinogen (Fig. 4B). Finally, the coiled-coil connectors showed a kink in the middle (Fig. 4B) corresponding to the crystallographically determined hinge of the triple-helices [35].

When fibrinogen was imaged on glass, mica, or APTES-modified mica, the molecules also had a characteristic trinodular shape, but the fine structural details such as the γ- and β-nodules, coiled-coil connectors and αC regions remained invisible (Fig. 4C–E). Therefore, GM-coated graphite was the only AFM substrate of the four tested that allowed for visualization and quantitative analysis of fine submolecular structural details of fibrinogen [38].

To compare the influence of AFM substrates on the natural spatial flexibility of adsorbed elongated fibrinogen molecules, we measured the angle θ between two symmetrical halves of the molecule as shown on Fig. 4F. Then, the conformational flexibility of fibrinogen was segregated into 3 categories based on the angular values: straight (170-180° angles), slightly bent (130-170°), and strongly bent (< 130°) conformations (Fig. 4G). Fibrinogen molecules adsorbed onto GM-coated graphite demonstrated a considerable flexibility with 58% of the molecules in the slightly bent conformation, 15% of strongly bent molecules, and 27% of straight molecules. Fibrinogen molecules on glass had a very similar distribution with a slight tendency towards less flexible molecules (61% slightly bent, 11% strongly bent, and 28% straight). On the surface of bare mica, a fraction of strongly bent fibrinogen molecules increased to 48% in good agreement with the previously published data [3,39]. Conversely, on the surface of APTES-mica, the rigid unbent molecules clearly dominated (56%), with only

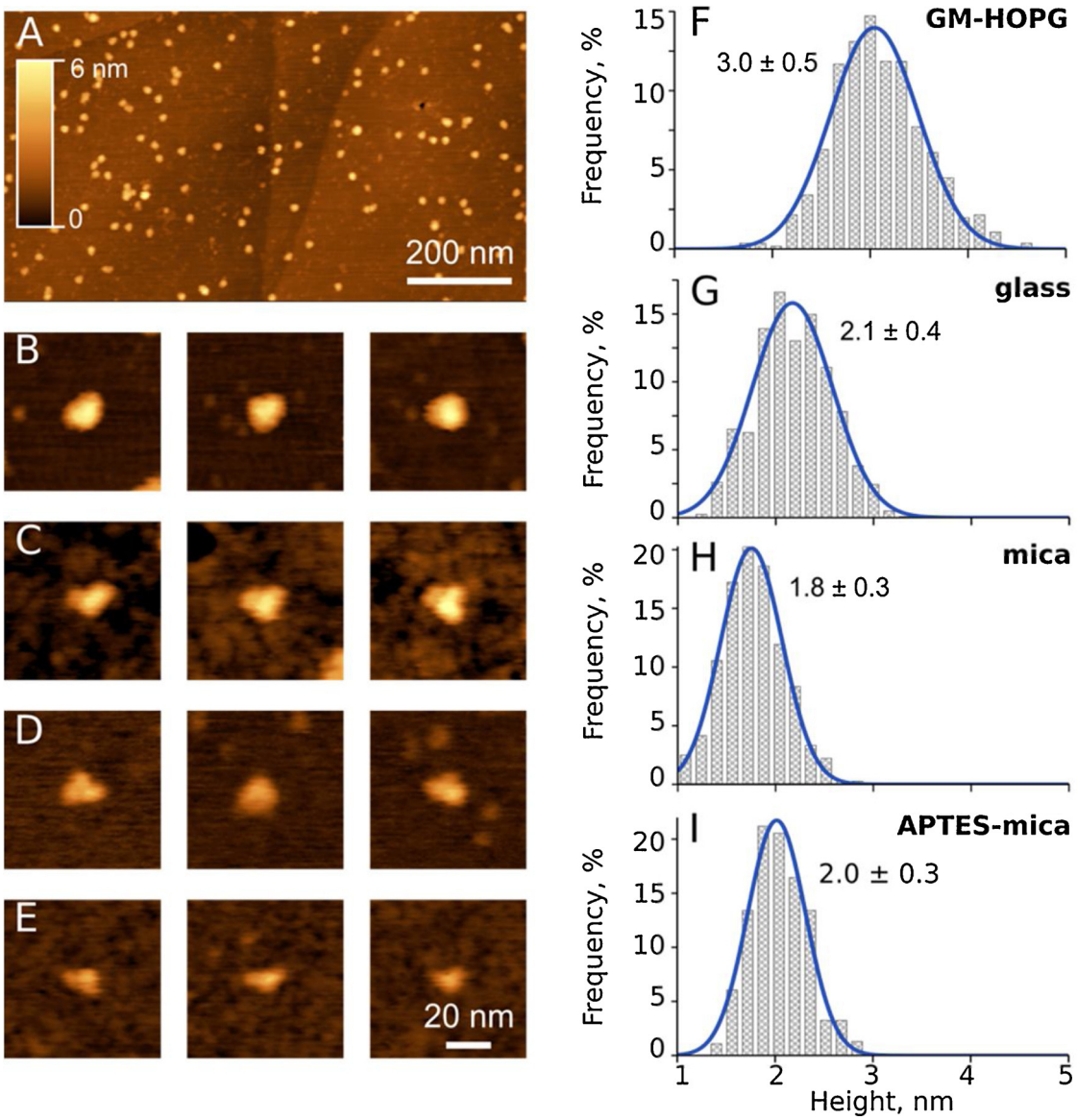

Fig. 3. Human IgG visualized with AFM on various substrates. (A) A representative low-resolution image of IgG on GM-coated graphite showing sparse single non-aggregated molecules. High-resolution images of individual IgG molecules on (B) GM-coated graphite, (C) glow-discharged glass, (D) freshly cleaved mica, and (E) mica modified with APTES. Height distributions of IgG molecules on (F) GM-coated graphite, sample size N = 557, (G) glow-discharged glass, N = 1228, (H) freshly cleaved mica, N = 360, and (I) mica modified with APTES, N = 462.

1% of strongly bent molecules seen on this surface. These data demonstrate that conformational flexibility of a protein revealed with AFM is strongly affected by the substrate used for protein adsorption and that the GM-coated graphite allows more of the natural conformational flexibility than other substrates analyzed, of which APTES-mica was the most restrictive.

To quantify the surface-related distortions of protein dimensions, we also measured the height of all three of fibrinogen's globular portions and analyzed them as multi-peak histograms. When adsorbed on GM-coated graphite, fibrinogen displayed the height distribution as three distinct peaks (Fig. 4H), of which the 2.9-nm peak corresponded to the terminal globules and two other peaks centered at 1.8 nm and 0.8 nm both corresponded to the central globule of fibrinogen and reflected its asymmetrical orientation on the surface. In fibrinogen molecules adsorbed on the other substrates tested, this spatial asymmetry remained undetectable and the corresponding height histograms had only two peaks (Fig. 4I–K). The heights of fibrinogen's globular portions were the largest on GM-coated graphite and closest to the corresponding dimensions in the crystal structure (about 5 and 3 nm for distal and central globules, respectively [35]) (Fig. 4H–I). These measurements confirm that on GM-coated graphite the 3D structure of the globular protein regions is preserved better than on the other substrates tested.

In summary, GM-coated graphite has advantages over other substrates used for AFM imaging of proteins in terms of smaller size distortions and higher conformational flexibility. It is also the only substrate that allowed us to directly observe unstructured protein regions such as fibrinogen αC regions, not visualized with other techniques, including AFM imaging on various substrates.

3.5. Use of GM-coated graphite for AFM of polyanions (heparin and DNA)

The surface of GM-coated graphite is positively charged at physiological pH, due to protonated amino groups on both ends of the modifier (Fig. 1). Therefore, negatively charged (polyanionic) biomacromolecules, such as sulphated glycosaminoglycans and nucleic acids, readily adsorb on GM-coated graphite via electrostatic interactions. Here we used heparin and double-stranded DNA to illustrate the

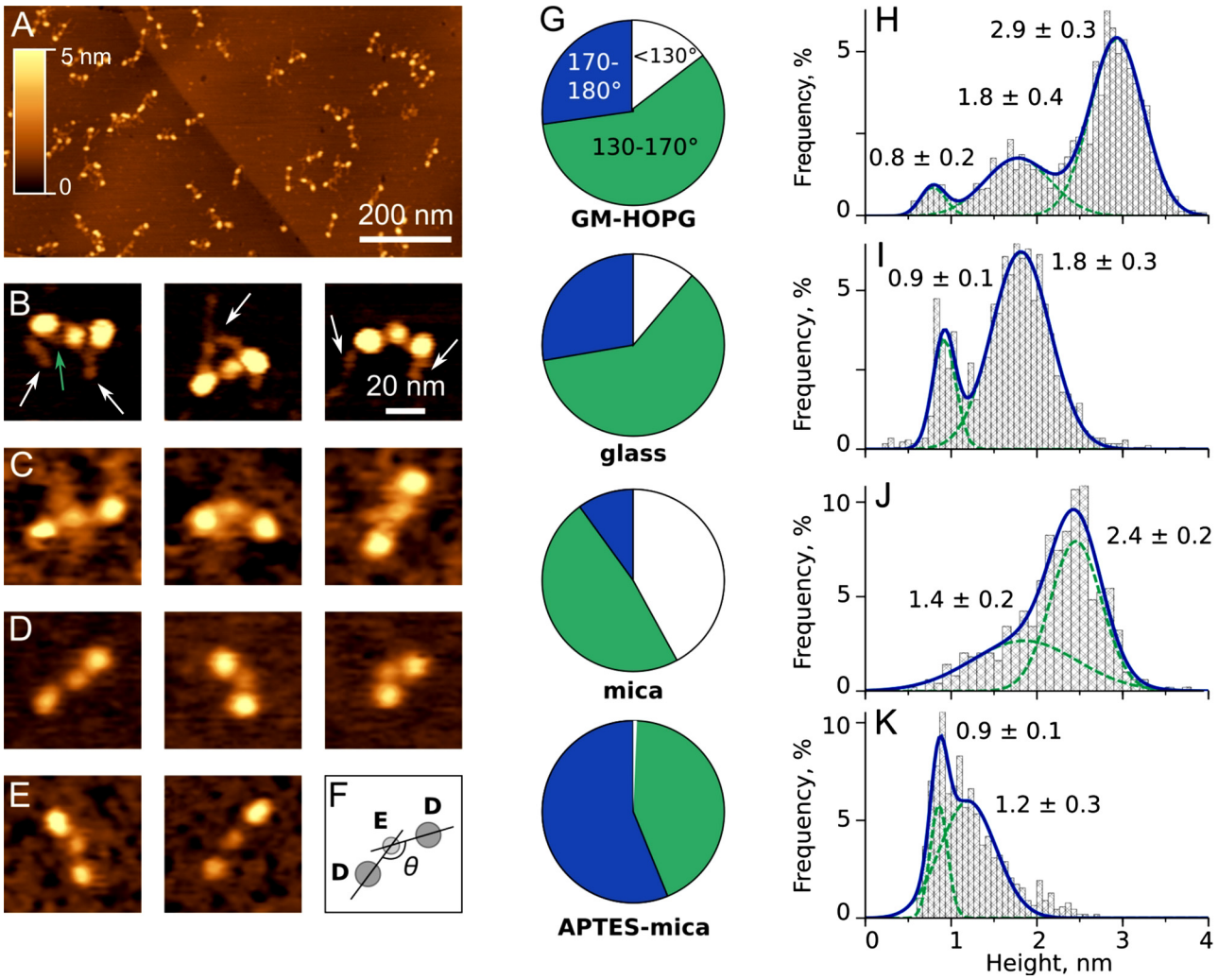

Fig. 4. Human fibrinogen visualized with AFM on various substrates. (A) A representative image of fibrinogen on GM-coated graphite. Individual fibrinogen molecules on (B) GM-coated graphite, (C) glow-discharged glass, (D) freshly cleaved mica, and (E) mica modified with APTES. White arrows in (B) point to the αC regions, a green arrow points to the kink in the coiled coil. (F) A diagram showing how the bending angle θ in the center of a molecule was measured in AFM images of fibrinogen. (G) Apparent flexibility of the fibrinogen molecules on various surfaces shown as variations of the angle θ. Each pie-chart shows the frequency of strongly bent (white), slightly bent (green) and straight molecules (blue); sample sizes on GM-coated graphite N = 302, on glass N = 314, on mica N = 101, on mica modified with APTES N = 324. Height distributions of fibrinogen on (H) GM-coated graphite, sample size N = 2654, (I) freshly cleaved mica, N = 497, (J) glow-discharged glass, N = 2162, and (K) mica modified with APTES, N = 1555.

application of GM-coated graphite for AFM of polyanionic biomolecules.

3.5.1. *Visualization of heparin*

Heparin is a natural anticoagulant, i. e. a substance that prevents blood clotting, which is widely used as a highly efficient medication to prevent and treat thrombosis. Structurally, heparin is a polymeric carbohydrate comprising a highly sulfated glycosaminoglycan with a varying molecular weight of 5-40 kDa in unfractionated preparations [40,41]. Heparin consists of a repeating disaccharide unit composed of a monosulfated iduronic acid and disulfated glucosamine. To the best of our knowledge, heparin has not been visualized with AFM or electron microscopy previously. A representative AFM image of unfractionated heparin on the GM-coated graphite (Fig. 5A) contained small elongated structures of various lengths with a mean height of 0.6 nm (Fig. 5B) and a contour length histogram with a peak at 14 nm (Fig. 5C). As expected for unfractionated heparin, which has a variety of sizes, the length distribution was lognormal with the longest heparin molecules stretched out to 40 nm and the shortest filaments having a length of about 7-8 nm. Comparison of our measurements with the previously estimated lengths of heparin molecules in solution determined by small-angle neutron scattering [42] suggests that the longest heparin molecules observed correspond to a molecular weight of 40 kDa, while the shortest ones could represent a molecular weight below 10 kDa. Thus, our imaging technique allows one to visualize, perform morphometry, and study conformations of polymeric carbohydrates at the single molecule level.

3.5.2. *Visualization of double-stranded DNA (dsDNA) and its complexes with anti-DNA antibodies*

DNA strands and DNA-protein complexes have been a traditional object of AFM studies [43,44]. Therefore, we explored if our modified substrate would provide competitive high-quality imaging of isolated dsDNA molecules and DNA-containing immune complexes. On the surface of GM-coated graphite, dsDNA was typically seen as long entangled threads (Fig. 6A) with an average height of 0.8 nm (Fig. 6B), while occasional stretches of melted single-stranded DNA had an average height of 0.4 nm. These dimensions are in good agreement with the previous AFM studies of double-stranded and single-stranded DNA [5,45].

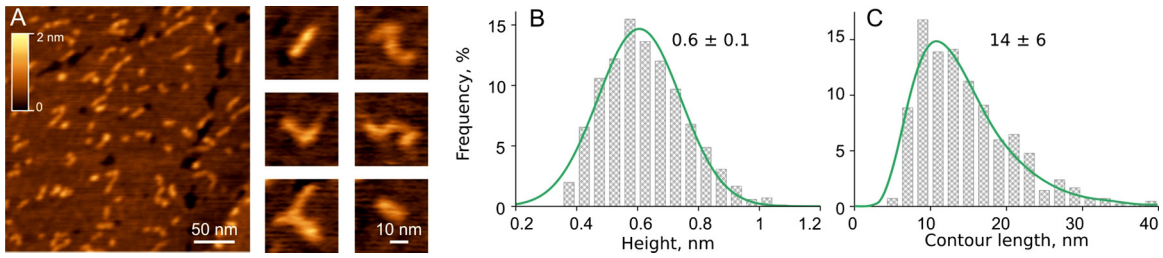

Fig. 5. AFM visualization of unfractionated heparin on GM-coated graphite. (A) Representative images with multiple (left) and individual (right) heparin molecules. (B) Height distribution of heparin molecules fitted with a Gaussian, N = 1557. (C) Lognormal distribution of the heparin contour lengths, N = 417.

Flexibility of DNA in solution and on the surface is characterized by its persistence length [46,47]. In solution, the DNA persistence length is dependent on environmental factors, such as temperature, ionic strength, etc. When DNA is adsorbed on a surface, the apparent persistence length changes, depending on the properties of the substrate and the mode of adsorption. Because positively charged surfaces, such as GM-coated graphite, adsorb DNA via kinetic trapping [5,48–50], we used this model to estimate the persistence length of the dsDNA in the FemtoScan Online software. DNA molecules were traced with polygonal chains, then a $\langle\theta^2(l)\rangle$ dependency was plotted, where $\langle\theta^2\rangle$ is an average square of the angle between two segments of the DNA separated by a contour length l from each other. The persistence length P was approximated from the slope of this plot using a formula $\langle\theta^2(l)\rangle = \frac{2l}{P}$. The persistence length of the dsDNA adsorbed on GM-coated graphite from a physiological solution at pH 7.4 containing 20 mM HEPES and 150 mM NaCl was equal to 32 nm, which is in good agreement with the solution-based measurements at a similar ionic strength [51].

In a similar way, GM-coated graphite could be used to image other types of DNA, such as single-stranded, triple-stranded, quadruplex DNA, and i-motif structures [45,52–54]. Generally, GM-graphite allows for the same quality of DNA imaging as other frequently used surfaces [25,45,52,55–59]. Both APTES-mica and GM-graphite trap DNA electrostatically, so its shape on the surface is best described by a 2D projection of a three-dimensional chain. In contrast, DNA molecules deposited on bare mica equilibrate on the surface and behave as ideal worm-like chains in two dimensions [48]. It could be expected that kinetic trapping will allow for visualization of DNA-protein complexes. To test that hypothesis, we further used dsDNA and human anti-dsDNA antibodies to illustrate that non-covalently bound molecular complexes can be also imaged with AFM using GM-coated graphite.

To generate DNA-antibody immune complexes, calf thymus dsDNA was diluted to 0.5 μg/ml and mixed with 0.1 μg/ml purified anti-dsDNA antibodies (final concentrations) in 20 mM HEPES buffer, pH 7.4. The mixture was incubated for 10 min at 37 °C before application to GM-coated graphite. Fig. 6C shows individual antibodies bound to one or two linear segments of the dsDNA. The characteristic Y-shape of the antibodies is clearly seen. Therefore, DNA-protein interactions are preserved during adsorption of their complexes to the surface of GM-coated graphite. We have also shown recently that other non-covalently bound protein complexes preserve their stoichiometry and tertiary structures after adsorption to GM-coated graphite [38,60].

Therefore, GM-coated graphite is suitable for visualization of polyanionic molecules, including sulphated glycosaminoglycans and DNA that adsorb on the GM-coated graphite via electrostatic interactions; they retain the conformations and intermolecular interactions similar to the ones observed in solution.

4. Conclusions

We present an improved methodology for single-molecule AFM imaging of biomacromolecules, including proteins, polysaccharides, and nucleic acids. The method is based on the use of a graphite surface coated with an amphiphilic modifier comprising a hydrophobic alkane hydrocarbon ($C_{10}H_{20}$) flanked by polar and positively charged tetraglycines on both ends of the molecule. The graphite modifier (GM) is water-soluble and the procedure of graphite modification is simple and fast. The modifier is applied to the surface of freshly cleaved graphite and within minutes it forms a uniform atomically smooth layer that improves substantially the AFM imaging of biomacromolecules. GM-coated graphite is much more hydrophilic than the bare graphite, positively charged at physiological pH, and thus adsorptive for various amphipathic, zwitterionic, and polyanionic molecules. GM-coated graphite has advantages over other traditional substrates used for AFM imaging in terms of higher resolution, smaller size distortions of individual protein molecules, and preservation of conformational flexibility of proteins and intermolecular protein-protein and DNA-protein interactions. The GM-coated graphite enabled us to produce high contrast images of flexible and/or unstructured protein regions that are difficult to visualize by other techniques. An additional advantage of GM-coated graphite is a high reproducibility of imaging. Therefore, application of GM-coated graphite for structural studies of disordered proteins has the potential to promote the use of high-resolution single-molecule AFM in structural biology.

5. Author Contributions

D. V. Klinov: developed the method of graphite modification, acquisition, analysis and interpretation of AFM data. A. D. Protopopova: concept and design, acquisition, analysis and interpretation of AFM data, writing. D. S. Andrianov: chemical synthesis, acquisition, analysis

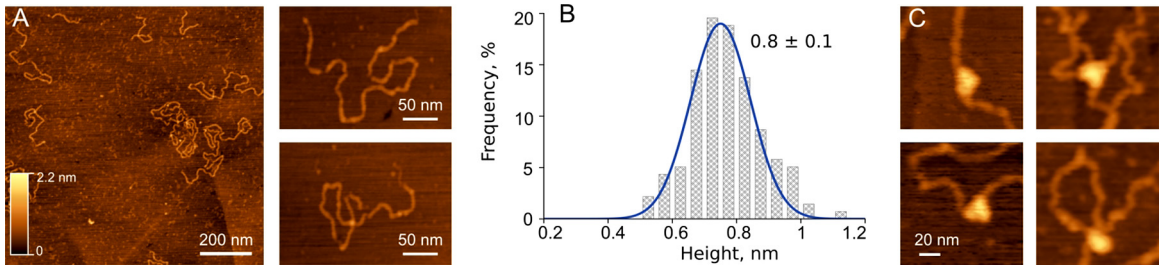

Fig. 6. AFM visualization of dsDNA and its complexes with anti-DNA antibodies. (A) Images of dsDNA and (B) distribution of height of dsDNA (N = 138). (C) Human anti-DNA IgG in complex with dsDNA.

and interpretation of NMR and mass spectrometry data, writing. R. I. Litvinov: concept and design, interpretation of data, writing. J. W. Weisel: concept and design, interpretation of data, writing. All authors have given approval to the final version of the manuscript.

Funding Sources

Funding was provided by NIH grants UO1-HL116330, RO1-HL135254, NSF grant DMR1505662, a Scholar Award from the American Society of Hematology, Russian Science Foundation grant 17-75-30064, bridge grant from the Perelman School of Medicine and by the Program for Competitive Growth at Kazan Federal University.

Declaration of Competing Interest

Nothing to disclose

ACKNOWLEDGMENT

We thank Dr. Russell Composto for providing access to an imaging system for water contact angle measurements, Dr. Sergei Vinogradov for help with chemical synthesis, and Izabella Andrianova for providing DNA-binding antibodies. Funding was provided by NIH grants UO1-HL116330, RO1-HL135254, NSF grant DMR1505662, a Scholar Award from the American Society of Hematology, Russian Science Foundation grant 17-75-30064, and by the Program for Competitive Growth at Kazan Federal University.

Appendix A. Supplementary data

Supplementary material related to this article can be found, in the online version, at doi:https://doi.org/10.1016/j.colsurfb.2020.111321.

References

[1] Y.F. Dufrêne, T. Ando, R. Garcia, D. Alsteens, D. Martinez-Martin, A. Engel, C. Gerber, D.J. Müller, Imaging modes of atomic force microscopy for application in molecular and cell biology, Nat. Nanotechnol. 12 (2017) 295–307, https://doi.org/10.1038/nnano.2017.45.

[2] S. Sheng, Y. Gao, A. Khromov, A.V. Somlyo, A.P. Somlyo, Z. Shao, Cryo-atomic force microscopy of unphosphorylated and thiophosphorylated single smooth muscle myosin molecules, J. Biol. Chem. 278 (2003) 39892–39896, https://doi.org/10.1074/jbc.M306094200.

[3] I.S. Yermolenko, V.K. Lishko, T.P. Ugarova, S.N. Magonov, High-resolution visualization of fibrinogen molecules and fibrin fibers with atomic force microscopy, Biomacromolecules. 12 (2011) 370–379, https://doi.org/10.1021/bm101122g.

[4] D.M. Czajkowsky, Z. Shao, The human IgM pentamer is a mushroom-shaped molecule with a flexural bias, Proc. Natl. Acad. Sci. 106 (2009) 14960–14965, https://doi.org/10.1073/pnas.0903805106.

[5] C. Rivetti, M. Guthold, C. Bustamante, Scanning force microscopy of DNA deposited onto mica: equilibration versus kinetic trapping studied by statistical polymer chain analysis, J. Mol. Biol. 264 (1996) 919–932, https://doi.org/10.1006/jmbi.1996.0687.

[6] Y.L. Lyubchenko, Preparation of DNA and nucleoprotein samples for AFM imaging, Micron. 42 (2011) 196–206, https://doi.org/10.1016/j.micron.2010.08.011.

[7] Y.L. Lyubchenko, L.S. Shlyakhtenko, Chromatin imaging with time-lapse atomic force microscopy, Methods Mol. Biol. 1288 (2015) 27–42, https://doi.org/10.1007/978-1-4939-2474-5.

[8] I.S. Chaschin, T.E. Grigorev, M.O. Gallyamov, A.R. Khokhlov, Direct deposition of chitosan macromolecules on a substrate from solutions in supercritical carbon dioxide: Solubility and conformational analysis, Eur. Polym. J. 48 (2012) 906–918, https://doi.org/10.1016/j.eurpolymj.2012.03.003.

[9] J. Moffat, V.J. Morris, S. Al-Assaf, A.P. Gunning, Visualisation of xanthan conformation by atomic force microscopy, Carbohydr. Polym. 148 (2016) 380–389, https://doi.org/10.1016/j.carbpol.2016.04.078.

[10] M. Kocun, M. Grandbois, L.A. Cuccia, Single molecule atomic force microscopy and force spectroscopy of chitosan, Colloids Surfaces B Biointerfaces. 82 (2011) 470–476, https://doi.org/10.1016/j.colsurfb.2010.10.004.

[11] J. Wang, S. Nie, Application of atomic force microscopy in microscopic analysis of polysaccharide, Trends Food Sci. Technol. 87 (2019) 35–46, https://doi.org/10.1016/j.tifs.2018.02.005.

[12] H.K. Christenson, Adhesion and surface energy of mica in air and water, J. Phys. Chem. 97 (1993) 12034–12041, https://doi.org/10.1002/9783527612451.ch34.

[13] V. Prokhorov, AFM observations of single polyolefin molecules on mica and graphite, in: K. Nitta (Ed.), Struct. Prop. Polyolefin Mater. Transworld Research Network, Kerala, India, 2012, pp. 53–96.

[14] N.A. Barinov, V.V. Prokhorov, E.V. Dubrovin, D.V. Klinov, AFM visualization at a single-molecule level of denaturated states of proteins on graphite, Colloids Surfaces B Biointerfaces. 146 (2016) 777–784, https://doi.org/10.1016/j.colsurfb.2016.07.014.

[15] C. Mücksch, H.M. Urbassek, Adsorption of BMP-2 on a hydrophobic graphite surface: a molecular dynamics study, Chem. Phys. Lett. 510 (2011) 252–256, https://doi.org/10.1016/j.cplett.2011.05.036.

[16] G. Raffaini, F. Ganazzoli, Protein adsorption on a hydrophobic surface: A molecular dynamics study of lysozyme on graphite, Langmuir 26 (2010) 5679–5689, https://doi.org/10.1021/la903769c.

[17] T. Svaldo-Lanero, A. Penco, M. Prato, M. Canepa, R. Rolandi, O. Cavalleri, Nanopatterning by protein unfolding, Soft Matter. 4 (2008) 965–967, https://doi.org/10.1039/b800621k.

[18] D.V. Klinov, L.P. Martynkina, V.Y. Yurchenko, V.V. Demin, S.A. Streltsov, Y.A. Gerasimov, Y.Y. Vengerov, Effect of SUPPorting substrates on the structure of DNA and DNA-trivaline complexes studied by atomic force microscopy, Russ. J. Bioorganic Chem. 29 (2003) 397–402 http://www.ncbi.nlm.nih.gov/pubmed/12947761.

[19] J.P. Rabe, S. Buchholz, Commensurability and mobility in two-dimensional molecular patterns on graphite, Science 253 (1991) 424–427, https://doi.org/10.1126/science.253.5018.424.

[20] E.V. Dubrovin, S. Speller, I.V. Yaminsky, Statistical analysis of molecular nanotemplate driven DNA adsorption on graphite, Langmuir 30 (2014) 15423–15432, https://doi.org/10.1021/la5041773.

[21] N. Severin, J. Barner, A.A. Kalachev, P. Rabe, Manipulation and overstretching of genes on solid substrates, Nano Lett. 4 (2004) 577–579, https://doi.org/10.1021/nl035147d.

[22] M. Bergkvist, J. Carlsson, S. Oscarsson, Surface-dependent conformations of human plasma fibronectin adsorbed to silica, mica, and hydrophobic surfaces, studied with use of atomic force microscopy, J. Biomed. Mater. Res. A. 64 (2003) 349–356, https://doi.org/10.1002/jbm.a.10423.

[23] N. Chada, K.P. Sigdel, R.R.S. Gari, T.R. Matin, L.L. Randall, G.M. King, Glass is a viable substrate for precision force microscopy of membrane proteins, Sci. Rep. 5 (2015) 1–8, https://doi.org/10.1038/srep12550.

[24] G. Le Minh, A.D. Peshkova, I.A. Andrianova, T.B. Sibgatullin, A.N. Maksudova, J.W. Weisel, R.I. Litvinov, Impaired contraction of blood clots as a novel prothrombotic mechanism in systemic lupus erythematosus, Clin. Sci. 132 (2018) 243–254, https://doi.org/10.1042/cs20171510.

[25] J. Adamcik, F. Valle, G. Witz, K. Rechendorff, G. Dietler, The promotion of secondary structures in single-stranded DNA by drugs that bind to duplex DNA: an atomic force microscopy study, Nanotechnology. 19 (2008) 384016, , https://doi.org/10.1088/0957-4484/19/38/384016.

[26] E.A. Obraztsova, D.V. Basmanov, N.A. Barinov, D.V. Klinov, Carbon Nanospikes: Synthesis, characterization and application for high resolution AFM, Ultramicroscopy 197 (2019) 11–15, https://doi.org/10.1016/j.ultramic.2018.11.004.

[27] I. Yaminsky, A. Akhmetova, G. Meshkov, Femtoscan online software and visualization of nano-objecs in high-resolution microscopy, Nanoindustry Russ. 11 (2018) 414–416, https://doi.org/10.22184/1993-8578.2018.11.6.414.416.

[28] D. V. Klinov, N. V. Bovin, Patent RU2305592C2: Method for modifying hydrophobic surfaces, RU2305592C2, 2007.

[29] M.H. Lee, D.A. Brass, R. Morris, R.J. Composto, P. Ducheyne, The effect of non-specific interactions on cellular adhesion using model surfaces, Biomaterials 26 (2005) 1721–1730, https://doi.org/10.1016/j.biomaterials.2004.05.026.

[30] Y. Wei, C.Q. Jia, Intrinsic wettability of graphitic carbon, Carbon N. Y. 87 (2015) 10–17, https://doi.org/10.1016/j.carbon.2015.02.019.

[31] C.A. Amadei, C.Y. Lai, D. Heskes, M. Chiesa, Time dependent wettability of graphite upon ambient exposure: The role of water adsorption, J. Chem. Phys. 141 (2014) 084709, , https://doi.org/10.1063/1.4893711.

[32] N.A. Barinov, A.D. Protopopova, E.V. Dubrovin, D.V. Klinov, Thermal denaturation of fibrinogen visualized by single-molecule atomic force microscopy, Colloids Surfaces B Biointerfaces. 167 (2018) 370–376, https://doi.org/10.1016/j.colsurfb.2018.04.037.

[33] E.O. Saphire, P.W.H.I. Parren, R. Pantophlet, M.B. Zwick, G.M. Morris, P.M. Rudd, R.A. Dwek, R.L. Stanfield, D.R. Burton, I.A. Wilson, Crystal structure of a neutralizing human IgG against HIV-1: A template for vaccine design, Science (80-.) 293 (2001) 1155–1159, https://doi.org/10.1126/science.1061692.

[34] J.W. Weisel, R.I. Litvinov, Fibrin formation, structure and properties, Subcell. Biochem. 82 (2017) 405–456, https://doi.org/10.1007/978-3-319-49674-0.

[35] J.M. Kollman, L. Pandi, M.R. Sawaya, M. Riley, R.F. Doolittle, Crystal structure of human fibrinogen, Biochemistry 48 (2009) 3877–3886, https://doi.org/10.1021/bi802205g.

[36] Y.I. Veklich, O.V. Gorkun, L.V. Medved, W. Nieuwenhuizen, J.W. Weisel, Carboxyl-terminal portions of the alpha chains of fibrinogen and fibrin, J. Biol. Chem. 268 (1993) 13577–13585.

[37] A.D. Protopopova, N.A. Barinov, E.G. Zavyalova, A.M. Kopylov, V.I. Sergienko, D.V. Klinov, Visualization of fibrinogen αC regions and their arrangement during fibrin network formation by high-resolution AFM, J. Thromb. Haemost. 13 (2015) 570–579, https://doi.org/10.1111/jth.12785.

[38] A.D. Protopopova, R.I. Litvinov, D.K. Galanakis, C. Nagaswami, N.A. Barinov, A.R. Mukhitov, D.V. Klinov, J.W. Weisel, Morphometric characterization of fibrinogen's αC regions and their role in fibrin self-assembly and molecular organization, Nanoscale 9 (2017) 13707–13716, https://doi.org/10.1039/C7NR04413E.

[39] S. Köhler, F. Schmid, G. Settanni, Molecular dynamics simulations of the initial adsorption stages of fibrinogen on mica and graphite surfaces, Langmuir 31 (2015)

13180–13190, https://doi.org/10.1021/acs.langmuir.5b03371.
[40] P.L. Walton, C.R. Ricketts, D.R. Bangham, Heterogeneity of heparin, Br. J. Haematol. 12 (1966) 310–325.
[41] G.H. Barlow, Molecular weight distribution determination on heparin samples, Thromb. Res. 31 (1983) 513–519.
[42] K.A. Rubinson, Y. Chen, B.F. Cress, F. Zhang, R.J. Linhardt, Heparin's solution structure determined by small-angle neutron scattering, Biopolymers 105 (2016) 905–913, https://doi.org/10.1002/bip.22936.
[43] Y.L. Lyubchenko, L.S. Shlyakhtenko, AFM for analysis of structure and dynamics of DNA and protein-DNA complexes, Methods 47 (2009) 206–213, https://doi.org/10.1016/j.ymeth.2008.09.002.
[44] E.C. Beckwitt, M. Kong, B. Van Houten, Seminars in Cell & Developmental Biology Studying protein-DNA interactions using atomic force microscopy, Semin. Cell Dev. Biol. 73 (2018) 220–230, https://doi.org/10.1016/j.semcdb.2017.06.028.
[45] J. Adamcik, D.V. Klinov, G. Witz, S.K. Sekatskii, G. Dietler, Observation of single-stranded DNA on mica and highly oriented pyrolytic graphite by atomic force microscopy, FEBS Lett. 580 (2006) 5671–5675, https://doi.org/10.1016/j.febslet.2006.09.017.
[46] A.A. Travers, The structural basis of DNA flexibility, Philos. Trans. A. Math. Phys. Eng. Sci. 362 (2004) 1423–1438, https://doi.org/10.1098/rsta.2004.1390.
[47] J. Bednar, P. Furrer, V. Katritch, A. Stasiak, J. Dubochet, A. Stasiak, Determination of DNA persistence length by cryo-electron microscopy. Separation of the static and dynamic contributions to the apparent persistence length of DNA, J. Mol. Biol. 254 (1995) 579–594, https://doi.org/10.1006/jmbi.1995.0640.
[48] A. Podestà, M. Indrieri, D. Brogioli, G.S. Manning, P. Milani, R. Guerra, L. Finzi, D. Dunlap, Positively charged surfaces increase the flexibility of DNA, Biophys. J. 89 (2005) 2558–2563, https://doi.org/10.1529/biophysj.105.064667.
[49] M. Joanicot, B. Revet, DNA conformational studies from electron microscopy. I. Excluded volume effect and structure dimensionality, Biopolymers 26 (1987) 315–326.
[50] F. Valle, M. Favre, P. De Los Rios, A. Rosa, G. Dietler, Scaling exponents and probability distributions of DNA end-to-end distance, Phys. Rev. Lett. 95 (2005) 1–4, https://doi.org/10.1103/PhysRevLett.95.158105.
[51] S. Brinkers, H.R.C. Dietrich, F.H. De Groote, I.T. Young, B. Rieger, The persistence length of double stranded DNA determined using dark field tethered particle motion, J. Chem. Phys. 130 (2009) 215105, , https://doi.org/10.1063/1.3142699.
[52] D. Klinov, B. Dwir, E. Kapon, N. Borovok, T. Molotsky, A. Kotlyar, High-resolution atomic force microscopy of duplex and triplex DNA molecules, Nanotechnology 18 (2007) 225102, , https://doi.org/10.1088/0957-4484/18/22/225102.
[53] A.M. Varizhuk, A.D. Protopopova, V.B. Tsvetkov, N.A. Barinov, V.V. Podgorsky, M.V. Tankevich, M.A. Vlasenok, V.V. Severov, I.P. Smirnov, E.V. Dubrovin, D.V. Klinov, G.E. Pozmogova, Polymorphism of G4 associates: From stacks to wires via interlocks, Nucleic Acids Res. 46 (2018) 8978–8992, https://doi.org/10.1093/nar/gky729.
[54] A.D. Protopopova, V.B. Tsvetkov, A.M. Varizhuk, N.A. Barinov, V.V. Podgorsky, D.V. Klinov, G.E. Pozmogova, The structural diversity of C-rich DNA aggregates: Unusual self-assembly of beetle-like nanostructures, Phys. Chem. Chem. Phys. 20 (2018) 3543, https://doi.org/10.1039/c7cp05380k.
[55] L. Hamon, D. Pastré, P. Dupaigne, C. Le Breton, E. Le Cam, O. Piétrement, High-resolution AFM imaging of single-stranded DNA-binding (SSB) protein-DNA complexes, Nucleic Acids Res. 35 (2007) e58, https://doi.org/10.1093/nar/gkm147.
[56] H.G. Hansma, I. Revenko, K. Kim, D.E. Laney, Atomic force microscopy of long and short nucleic acids, Nucleic Acids Res. 24 (1996) 713–720, https://doi.org/10.1093/nar/24.4.713.
[57] A. Kotlyar, N. Borovok, T. Molotsky, D. Klinov, B. Dwir, E. Kapon, Synthesis of novel poly(dG)-poly(dG)-poly(dC) triplex structure by Klenow exo- fragment of DNA polymerase I, Nucleic Acids Res. 33 (2005) 6515–6521, https://doi.org/10.1093/nar/gki963.
[58] A. Kotlyar, N. Borovok, T. Molotsky, H. Cohen, E. Shapir, D. Porath, Long, monomolecular guanine-based nanowires, Adv. Mater. 17 (2005) 1901–1905, https://doi.org/10.1002/adma.200401997.
[59] T.C. Marsh, J. Vesenka, E. Henderson, A new DNA nanostructure, the G-wire, imaged by scanning probe microscopy, Nucleic Acids Res. 23 (1995) 696–700, https://doi.org/10.1093/nar/23.4.696.
[60] A.D. Protopopova, A. Ramirez, D.V. Klinov, R.I. Litvinov, J.W. Weisel, Factor XIII topology: organization of B subunits and changes with activation studied with single-molecule atomic force microscopy, J. Thromb. Haemost. 17 (2019) 737–748, https://doi.org/10.1111/jth.14412.